

1 **Multiple scattering correction factor of quartz filters and the effect of filtering particles**
2 **mixed in water: implications to analyses of light-absorption in snow samples**

3
4 Jonas Svensson^{1*}, Johan Ström², and Aki Virkkula¹

5
6 ¹Atmospheric Composition Research, Finnish Meteorological Institute, Helsinki, Finland

7 ²Department of Environmental Science and Analytical Chemistry, Stockholm University,
8 Stockholm, Sweden

9 *Now at Institute for Geosciences and Environmental Research, University of Grenoble
10 Alpes, Grenoble, France

11
12 *Correspondence to J. Svensson (jonas.svensson@fmi.fi)*

13
14 **Abstract**

15 The deposition of light-absorbing aerosols (LAA) onto snow initiates processes that lead to increased
16 snowmelt. Measurements of LAA, such as black carbon (BC) and mineral dust, have been observed
17 globally to darken snow. Several measurement techniques of LAA in snow collect the particulates on
18 filters for analysis. Here we investigate micro-quartz filters optical response to BC experiments where
19 the particles initially are suspended in air or in a liquid. With particle soot absorption photometers
20 (PSAP) we observed a 20% scattering enhancement for quartz filters compared to the standard PSAP
21 Pallflex filters. The multiple-scattering correction factor (C_{ref}) of the quartz filters for airborne soot
22 aerosol is estimated to ~ 3.4 . In the next stage correction factors were determined for BC particles mixed
23 in water and also for BC particles both mixed in water and further treated in an ultrasonic bath.
24 Comparison of BC collected from airborne particles with BC mixed in water filters indicated
25 approximately a factor of two higher mass absorption cross section for the liquid based filters, probably
26 due to the BC particles penetrating deeper in the filter matrix. The ultrasonic bath increased absorption
27 still further, roughly by a factor of 1.5 compared to only mixing in water. Application of the correction
28 functions to earlier published field data from the Himalaya and Finnish Lapland yielded MAC values
29 of $\sim 7 - 10 \text{ m}^2 \text{ g}^{-1}$ at $\lambda = 550 \text{ nm}$ which is in the range of published MAC of airborne BC aerosol.

30
31 **1 Introduction**

32 Soot **refers to carbonaceous particles formed during the incomplete combustion of hydrocarbon fuels,**
33 **and includes black carbon (BC) and organic carbon (OC), but can also include other elements, such as**
34 **sulfates.** ~~consists of black carbon (BC) and organic carbon (OC) particles formed during the incomplete~~
35 ~~combustion of carbonaceous fuels.~~ As the most light-absorbing aerosol (LAA) by unit per mass, BC is

36 highly efficient in absorbing solar radiation, and is a vital component in Earth's radiative balance (Bond
37 et al., 2013). Once the particles are scavenged from the atmosphere, possibly far from their emission
38 source, BC can reach a snow surface and decrease the snow reflectivity (Warren and Wiscombe, 1980;
39 Flanner et al., 2007). This will lead to accelerated and increased snowmelt, observed in different snow
40 environments across the globe (see e.g. recent review by Skiles et al., 2018). Perhaps most notably is
41 High Mountain Asia and its extensive cryosphere, where large emission sources of LAA in close
42 proximity is affecting the region's snow and ice (e.g. Xu et al., 2009; Gertler et al., 2016; Zhang et al.,
43 2017).

44

45 ~~There are a variety of methods for measuring BC~~ Measurements of BC consists of a variety of methods,
46 which is reflected in BC being operationally defined. A common practice is to measure the change in
47 transmission of a filter collecting aerosol. The measured signal (i.e. optical depth of the filter) is
48 thereafter applied with correction factors to generate atmospheric concentrations of so-called equivalent
49 black carbon (eBC) according to the BC nomenclature (Petzold et al., 2013). The correction factors
50 account for: 1) the loading of aerosol on the filter since the detection signal decreases with increased
51 aerosol content; 2) the multiple scattering of light that is enhanced in the filter substrate; 3) and the
52 enhancement from the deposition of other light scattering aerosol. One instrument used for light
53 absorption measurements is the Particle Soot Absorption Photometer (PSAP), utilizing Pallflex filters.
54 As an alternative for the optical filter analysis of eBC, another approach is to apply the thermal-optical
55 method (TOM), providing organic carbon (OC) and elemental carbon (EC) mass of the aerosol on the
56 filter. With this method, EC refers to the carbon content of carbonaceous matter (Petzold et al., 2013),
57 and can be assumed to be the main light-absorbing element of BC. The technique involves a stepwise
58 heating procedure, therefore creating a need to use micro quartz fiber filters. These filters have been
59 used in numerous studies with filtering snow and ice samples, and thereafter analyzed to determine the
60 EC and OC content of the samples (e.g. Hagler et al., 2007; Forsström et al., 2009; Meinander et al.,
61 2013; Ruppel et al., 2014; Zhang et al., 2017). In Svensson et al. (2018), measurements with TOM were
62 combined with an additional transmittance measurement to further characterize the LAA present on the
63 filter samples investigate the relative contribution from BC and other LAA particles present in snow
64 samples. The study involved laboratory tests, as well as comparisons to ambient snow samples taken
65 from different environmental settings. One lesson from this study was that the optical properties of
66 absorbing particles on quartz filters must be better understood. In particular when using melted snow
67 samples.

68

69 The overarching goal of this paper is to further investigate micro quartz fiber filters optical behavior
70 when sampling BC particles in a liquid (to simulate snow sampling). An advantage of using these filter
71 is that the sample can be analysed readily using TOM to arrive to an EC concentration on the filter
72 (where MAC values are not needed). This aim is pursued through a series of laboratory studies of BC

73 filter deposition in an airborne phase, as well as when the same BC particles are mixed in water and
74 filtered onto the quartz filters (to simulate snow sampling). Our approach is to compare the use of quartz
75 fibre filter for air and liquid samples to the much better characterized pallflex type filter used in
76 commercial PSAPs. Hence, we are not intending to determine a universal MAC value, but rather to
77 understand differences in the observations that might be due to the filter substrate or handling of the
78 sample. We do not intend to answer all possible issues with filter sampling, but will concentrate on the
79 difference using the two filter types in air samples, the difference between air and liquid samples with
80 respect to the quartz fibre filter, and finally the potential effect from treating the liquid samples using
81 ultrasound.

82

83 **2 Materials, instruments, and data analyses**

84 **2.1 Soot aerosol production and sampling**

85 A schematic picture of the experiment is presented in Fig. 1, and the methods used in each step are
86 outlined in the subsections (2.1.1 and 2.1.2) below, as well as the instrumentation used (sections under
87 2.2). Section 2.3 explains the data processing. The soot used consisted of particles collected by chimney
88 cleaners in Helsinki, Finland, and this particular soot batch is from small-scale oil-based burning. The
89 same soot has been applied in different experiments previously (Peltoniemi et al., 2015; Svensson et
90 al., 2016; 2018).

91

92 **2.1.1 Airborne sampling**

93 Soot aerosol were sampled onto filters in an airborne phase and as a part of liquid solution. In the
94 airborne aerosol tests, soot was blown into a cylindrical experimental chamber (0.8 m height \times 0.45 m
95 diameter) through a stainless steel tube (25 mm outer diameter) consisting of a y-shaped bend of 130°,
96 creating a size-separation of the aerosol. Essentially a virtual impactor, this set-up allowed the smaller
97 sized particles to continue with the airflow into the chamber, while the larger (and heavier) particles
98 were deposited into a waste pipe through inertial separation (see section 2.2.3 for further description
99 and results in section 3.1.1.).~~The soot used consisted of particles collected by chimney cleaners in~~
100 ~~Helsinki, Finland, and this particular soot batch is from small scale oil based burning. The same soot~~
101 ~~has been applied in experiments previously (Peltoniemi et al., 2015; Svensson et al., 2016; Svensson et~~
102 ~~al., 2018).~~ From the experimental chamber a sample inlet (copper, 6 mm outer diameter) simultaneously
103 fed two PSAPs and a portable aerosol spectrometer (Grimm 1.108). One of the PSAPs had quartz fiber
104 filter punches mounted, while the other had standard PSAP filters installed. This set-up was alternated
105 among the PSAPs in between the experimental runs during the experiment, to have both PSAPs assessed
106 with the different filters. In total, 22 different experimental rounds were made with various amounts of
107 aerosol deposited to the substrates.

108

109 **2.1.2 Liquid sampling**

110 In the liquid experiments, the same soot batch and procedure were used as above, but the outlet pipe
111 was submerged into a 20 L container filled with deionized, purified Milli-Q (MQ) water. From this
112 liquid solution, different small amounts (between 10-100 mL) were extracted and mixed with additional
113 MQ water to further dilute the sample (to a typical total volume of 400 mL). This was performed to get
114 a range of filters with different EC concentrations and optical depths. The total number of liquid-
115 generated filters was 35. Some selected liquid samples (n=10) were exposed to an ultrasonic bath (for
116 at least 15 mins) prior to filtration ~~to further mix the soot solutions~~. All of the liquid solutions were
117 filtered onto the same quartz filters used in the airborne test, applying the same filtering principles and
118 analysis procedures as used previously (Svensson et al., 2018). Punches from dried filters had their
119 transmittance first measured using a PSAP, followed by EC concentration measurements (TOM). This
120 procedure was also applied to the quartz filters from the airborne experiment.

121

122 **2.2 Instruments**

123 **2.2.1 Absorption measurements**

124 Absorption was measured with two Radiance Research 3-wavelength PSAPs (S/N 90 and S/N 100) at
125 $\lambda=467$ nm, 530 nm, and 660 nm (Virkkula et al., 2005). One of them was loaded with Pallflex E70-
126 2075W filter that is generally used with the instrument, while the other was loaded with micro quartz
127 fiber filters (Munktell, grade T293). The flows were calibrated with a Gilian Gilibrator bubble flow
128 meter and set to 0.5 LPM. Higher flow rates were not used here since the quartz filter tends to be more
129 fragile and may not withstand higher flows. The sample spot diameters of the PSAPs were measured
130 with an Eschenbach scale loupe with a 0.1 mm graduation ten times each. The average diameters (\pm
131 standard deviation) were 5.04 ± 0.10 mm and 5.05 ± 0.10 mm, giving corresponding spot areas of 19.9
132 ± 1.6 mm² and 20.0 ± 1.6 mm². The aim was to use identical face velocities, i.e. average velocity of
133 aerosol perpendicular to the filter (e.g. Müller et al., 2014) through both filter materials. The essentially
134 identical spot areas meant also that we had tuned the flow rates identical. In addition, to study whether
135 the PSAPs themselves affect the results we used both filter materials alternatingly, as mentioned above,
136 resulting in half of the 22 quartz filter samples being collected on the PSAP S/N 100, and the other half
137 on the PSAP S/N 90. Another custom-built 1-wavelength PSAP ($\lambda=526$ nm; Krecl et al., 2007) used in
138 Svensson et al (2018), was also utilized in for transmittance analysis of all the filters after their
139 production in the airborne- and liquid experiments.

140

141 **2.2.2 EC measurements**

142 Punches (typically with an area of 0.64 cm²) taken from the quartz filters were determined for their OC
143 and EC content with a Sunset Laboratory OCEC-analyzer (Birch and Cary, 1996), using the
144 EUSAAR_2 protocol (Cavalli et al., 2010). The analysis procedure is based on step-wise increases in
145 temperature in a helium atmosphere for the first stage, during which OC is detected with a flame
146 ionization detector. The second phase of the analysis consists of introducing oxygen into the
147 temperature increases and the detection of EC. Pyrolysis of OC during the first phase is monitored by a
148 continuous laser transmittance measurement. Once the transmittance has reached the initial value for
149 the filter in the second phase, a separation split-point between OC and EC is established.

150

151 **2.2.3 Size distribution measurements**

152 During the airborne experiments a Grimm optical particle counter (OPC, 1.108) was used as a portable
153 aerosol spectrometer for particle size distributions. The OPC have been factory-calibrated with PSL
154 spheres that are white. Their scattering cross section is larger than that of BC particles which leads to
155 underestimation of particle diameter. We did not find published Grimm 1.108 calibrations with BC
156 particles in the literature, thus we approximated the effect. By using the cross sections modeled by
157 Rosenberg et al. (2012) we estimate that the diameters presented by the OPC are possibly lower by a
158 factor of 2. In Figure 2 we present both the original size distributions and those calculated by
159 multiplying the diameters by 2.

160

161 **2.3 Data processing**

162 Calculations are presented in a step-by-step procedure below. Loading corrections are routinely applied
163 to filter-based measurements of light absorption by atmospheric aerosol, but, for measurements of
164 absorption by melted and filtered snow samples it is not. In the former, absorption is calculated from
165 the product of a loading correction and the rate of change of transmittance, whereas in the latter the
166 absorption is generally calculated simply from the transmittance of the filter only. We therefore show
167 the equivalence of the two methods and that the loading corrections can and should be applied also to
168 melted and filtered snow samples. First, we present a generally use equation for calculating absorption
169 by aerosols, then how the multiple scattering correction factor C_{ref} appears in the equations, followed
170 by how we determined it for the quartz filters. The numerical values of two published loading
171 corrections are given as clearly as possible to save the reader from looking for constants from the
172 literature. Finally, we show the equivalence of calculating the mass absorption coefficients from
173 airborne aerosol and filtered snow samples.

174

175 A further note on data processing is important. The single-scattering albedo, ω_0 , i.e. the ratio of
 176 scattering and extinction coefficient, is a measure of the darkness of aerosols: for purely scattering
 177 aerosols $\omega_0 = 1$. For freshly-generated pure BC, it has been measured to be $\sim 0.2 \pm 0.1$ (Bond et al. 2013).
 178 When pure BC particles get coated with some light-scattering material ω_0 increases so that far from the
 179 sources it is typically larger than 0.9 (e.g., Delene and Ogren, 2002). However, ω_0 varies also with
 180 particle size even for pure BC, in a way that it increases with increasing particle size as can be shown
 181 by the simple Mie calculations in Fig 2b. Both the coating and particle size have consequences for the
 182 analysis of BC in snow by filter-based absorption measurements. The coating of BC particles typically
 183 consists of some water-soluble material such as sulfates, nitrates and organics. The size of BC particles
 184 in snow has been shown to vary in a large range from $\sim 0.1 \mu\text{m}$ to $> 2 \mu\text{m}$ (e.g., Schwarz et al., 2013).
 185 On the other hand, the estimation of absorption from filter-based attenuation measurements is affected
 186 also by scattering aerosol and therefore by ω_0 (e.g., Arnott et al., 2005; Virkkula et al., 2005; Collaud
 187 Coen et al, 2010). Now, since we do not know the ω_0 of the particles and we will apply the algorithm
 188 presented by Virkkula (2010) we will repeat the calculations with four different ω_0 values. We use the
 189 size distribution measurements for estimating the size and the Mie modeling for estimating a realistic
 190 range of ω_0 for the calculations.

191

192 2.3.1 Calculation of absorption in aerosols

193 The PSAP has been calibrated with the standard filter material Pallflex E70-2075W by Bond et al.
 194 (1999; here referred to as B1999) and Virkkula et al. (2005). Ogren (2010; here O2010) presented an
 195 adjustment to the Bond et al. (1999) calibration, while Virkkula (2010; here V2010) updated the
 196 Virkkula et al. (2005) calibration. In all of these the absorption coefficient is calculated as

$$197 \quad \sigma_{op} = f(Tr_t) \frac{A}{Q\Delta t} \ln \left(\frac{Tr_{t-\Delta t}}{Tr_t} \right) - s\sigma_{sp} \quad (1)$$

198 where $f(Tr_t)$ is the loading correction function that depends on the transmittance $Tr_t = I_t/I_0$ where I_t is
 199 the light intensity transmitted through the filter at time t, I_0 the light intensity transmitted through a
 200 clean filter at time t = 0, A the spot area, Q the flow rate, and s the fraction of the scattering coefficient
 201 σ_{sp} that gets interpreted as absorption and gets usually called the apparent absorption and should be
 202 subtracted from the uncorrected absorption or be treated as presented by Müller et al. (2014). If apparent
 203 absorption can be considered negligible, equation 1 becomes

$$204 \quad \sigma_{op} = f(Tr_t) \frac{A}{Q\Delta t} \ln \left(\frac{Tr_{t-\Delta t}}{Tr_t} \right) \quad (2)$$

205 In the present work, this approach was adapted for two reasons: 1) σ_{sp} was not measured during the
 206 calibration experiment and 2) the aerosol used in the experiment was very dark (soot from oil-based
 207 burning), thus the apparent absorption could be considered negligible.

208

209 The loading correction function $f(\text{Tr})$ can be further rewritten as $f(\text{Tr}) = g(\text{Tr})/C_{\text{ref}}$ where C_{ref} is the
 210 multiple scattering correction factor and $g(\text{Tr})$ at $\text{Tr} = 1$ a loading correction function that equals one at
 211 $\text{Tr} = 1$ and increases when the filter gets darker, i.e., when $\text{Tr} < 1$.

$$212 \quad \sigma_{\text{ap}} = \frac{1}{C_{\text{ref}}} g(\text{Tr}_t) \frac{A}{Q\Delta t} \ln\left(\frac{\text{Tr}_{t-\Delta t}}{\text{Tr}_t}\right) \quad (3)$$

213 If there is only one time step $t = \Delta t$ and before sampling $\text{Tr} = 1$ then $\text{Tr}_{t-\Delta t} = \text{Tr}_{t=0} = 1$ and

$$214 \quad \sigma_{\text{ap}} = \frac{1}{C_{\text{ref}}} g(\text{Tr}_t) \frac{A}{V_t} \ln\left(\frac{1}{\text{Tr}_t}\right) = \frac{1}{C_{\text{ref}}} g(\text{Tr}_t) \sigma_0 \quad (4)$$

215 where V_t is the air volume drawn through the filter since the start of sampling at time t . The assumption
 216 of only one time step means (4) presents the absorption coefficient since the start of sampling on the
 217 filter. According to the Bouguer-Lambert-Beer law light intensity decreases exponentially as a function
 218 of the optical depth τ

$$219 \quad \begin{aligned} I_t &= I_0 e^{-\tau} \\ \Leftrightarrow \tau &= \ln\left(\frac{I_0}{I_t}\right) = \ln\left(\frac{1}{\text{Tr}_t}\right) \end{aligned} \quad (5)$$

220 This is relevant especially in the present study since the purpose is to improve estimation of absorption
 221 in filtered snow samples. In the analysis of a snow sample there is only one "time step": I_0 is the intensity
 222 of light transmitted through a clean filter and I_t the intensity of light transmitted through a filter through
 223 which the melted snow sample has been filtered. Here the airborne data were also treated in a similar
 224 way: for each time step absorption was calculated from (4) since the start of sampling on the filter.

225

226 2.3.2 Calculation of C_{ref} of quartz filters

227 Comparison of the $\sigma_{\text{ap}}(\text{quartz}) (= \sigma_{\text{ap}}(\text{Q}))$ and $\sigma_{\text{ap}}(\text{Pallflex}) (= \sigma_{\text{ap}}(\text{P}))$ and keeping the published PSAP
 228 calibration functions (B1999, O2010, and V2010) as standards for $\sigma_{\text{ap}}(\text{P})$ we derive C_{ref} for the quartz
 229 filter by the following reasoning. If the same function $g(\text{Tr})$ is used for calculating both $\sigma_{\text{ap}}(\text{Q})$ and
 230 $\sigma_{\text{ap}}(\text{P})$ and especially if the same $C_{\text{ref}} = C_{\text{ref,P}}$ of the Pallflex filter is used for both filter materials the
 231 ratio of the absorption coefficients at time t is

$$232 \quad \frac{\sigma_{\text{ap}}(\text{Q}, C_{\text{ref,P}})}{\sigma_{\text{ap}}(\text{P}, C_{\text{ref,P}})} = \frac{\frac{1}{C_{\text{ref,P}}} g(\text{Tr}_Q) \frac{A}{V_t} \tau_Q}{\sigma_{\text{ap}}(\text{P}, C_{\text{ref,P}})} \quad (6)$$

233 If this ratio $\neq 1$ and if it is assumed that this is only due to using the same C_{ref} for both filter materials,
 234 in other words if using filter material dependent C_{ref} yielded equal absorption $\sigma_{\text{ap}}(\text{Q}, C_{\text{ref,Q}}) = \sigma_{\text{ap}}(\text{P}, C_{\text{ref,P}})$
 235 then

$$\begin{aligned}
 & \frac{\sigma_{ap}(Q, C_{ref,P})}{\sigma_{ap}(P, C_{ref,P})} = \frac{1}{C_{ref,P}} \frac{g(Tr_Q) \frac{A}{V_t} \tau_Q}{\sigma_{ap}(P, C_{ref,P})} = \frac{C_{ref,Q}}{C_{ref,P}} \frac{1}{C_{ref,Q}} \frac{g(Tr_Q) \frac{A}{V_t} \tau_Q}{\sigma_{ap}(P, C_{ref,P})} = \frac{C_{ref,Q}}{C_{ref,P}} \frac{\sigma_{ap}(Q, C_{ref,Q})}{\sigma_{ap}(P, C_{ref,P})} = \frac{C_{ref,Q}}{C_{ref,P}} \\
 & \Leftrightarrow C_{ref,Q} = \frac{\sigma_{ap}(Q, C_{ref,P})}{\sigma_{ap}(P, C_{ref,P})} C_{ref,P} \quad (7)
 \end{aligned}$$

which means $C_{ref,Q}$ is obtained simply by multiplying $C_{ref,P}$ with the observed ratio of the absorption coefficients.

If we assume that the difference of the absorption coefficients of the PSAPs using the quartz and Pallflex filters, $\sigma_{ap}(Q)$ and $\sigma_{ap}(P)$, respectively, is due to the multiple scattering correction factors of the two materials only we can calculate

$$C_{ref,Q} = \frac{\sigma_{ap}(Q)}{\sigma_{ap}(P)} C_{ref,P} \quad (6)$$

where $C_{ref,Q}$ and $C_{ref,P}$ are the multiple scattering correction factors of the quartz and Pallflex filters, respectively. However, this is an approximation only since the difference of $\sigma_{ap}(Q)$ and $\sigma_{ap}(P)$ is also due to the different transmittances Tr_Q and Tr_P of the two filter materials at each time step and consequently different values of the loading correction. However, below we will use (6) for the estimation of $C_{ref,Q}$.

The $C_{ref,P}$ values for Pallflex E70-2075W filter were calculated here from two published calibration experiments. The loading correction function of B1999 (with the O2010 adjustment) can be reformulated as

$$f(Tr) = \frac{1}{1.5557 \cdot Tr + 1.0227} \quad (87)$$

This can be further rewritten as

$$f(Tr) = \frac{1}{C_{ref}} g(Tr) = \frac{1}{2.5784} \frac{1}{0.6034 \cdot Tr + 0.3966} \quad (98)$$

where $C_{ref} = 2.5784$. Similarly, the V2010 loading correction can be rewritten as

$$\begin{aligned}
 f(Tr) &= (k_0 + k_1(h_0 + h_1 \omega_0) \ln(Tr)) = k_0 \left(1 + \frac{k_1}{k_0} (h_0 + h_1 \omega_0) \ln(Tr) \right) \\
 &= \frac{1}{C_{ref}} g(Tr) = \frac{1}{C_{ref}} \left(1 + \frac{k_1}{k_0} (h_0 + h_1 \omega_0) \ln(Tr) \right) \quad (109)
 \end{aligned}$$

where h_0 , h_1 , k_0 , and k_1 are the constants presented in Table 1 in V2010 and the single-scattering albedo $\omega_0 = \sigma_{sp}/(\sigma_{sp} + \sigma_{ap})$. For the three wavelengths (10) becomes

$$f_{467}(Tr_{467}) = \frac{1}{2.653} (1 - 1.698(1.16 - 0.63 \cdot \omega_0) \ln(Tr_b))$$

$$(110)$$

$$f_{530}(Tr_{530}) = \frac{1}{2.793} (1 - 1.788(1.17 - 0.71 \cdot \omega_0) \ln(Tr_g))$$

$$(121)$$

$$f_{660}(Tr_{660}) = \frac{1}{2.841} (1 - 1.915(1.14 - 0.72 \cdot \omega_0) \ln(Tr_r))$$

$$(132)$$

with $C_{ref,467} = 2.653$, $C_{ref,530} = 2.793$, and $C_{ref,660} = 2.841$.

When C_{ref} has been determined it is assumed that $g(Tr)$ is the same for both filter materials.

268

2.3.3 Calculation of mass absorption coefficient (MAC)

If m_{EC} is the mass of EC in the filter (corresponding to the spot area) through which the air volume of V_t has flown the average mass concentration of EC in aerosol in the air volume is $c_{EC,aerosol} = m_{EC}/V_t$. If σ_{ap} is the absorption coefficient calculated from (4), the mass absorption coefficient (MAC) can be calculated from

$$MAC = \frac{\sigma_{ap}}{c_{EC,aerosol}} = \frac{\frac{1}{C_{ref}} g(Tr_t) \frac{A}{V_t} \tau}{\frac{m_{EC}}{V_t}} = \frac{\frac{1}{C_{ref}} g(Tr_t) A \tau}{m_{EC}} = \frac{\frac{1}{C_{ref}} g(Tr_t) \tau}{\frac{m_{EC}}{A}} = \frac{f(Tr_t) \tau}{m_{EC}/A} \quad (143)$$

This applies for aerosol but also for the snow samples since the analysis of EC mass in a filter yields the mass surface density m_{EC}/A in where m_{EC} is the mass of EC in the analyzed filter spot that has the area A . In Svensson et al. (2018) we calculated apparent MAC values of EC in snow samples simply from $MAC = \tau/(m_{EC})$ without applying additional corrections for filter loading, neither enhanced absorption by the filter medium, nor light scattering particles. Assuming that only loading and filter effects apply in the experiments presented here, the apparent MAC values presented were adjusted by using $f(Tr,Q) = g(Tr)/C_{ref}Q(\Theta)$.

282

3 Results and discussion

3.1 Airborne aerosol experiment

Through our 22 airborne aerosol samples, we aimed at getting a range of transmittances and EC concentrations in the filters for the regression analysis. The original goal was to control the final transmittances by the length of the sampling time, however, this was not always successful (as noted in Table 1). Without dilution the aerosol concentration in the mixing chamber was very high with attenuation coefficients σ_0 in the range of $\sim 60000 - \sim 90000 \text{ Mm}^{-1}$ (see samples 1 and 2, Table 1). Therefore we added a dilution valve (V1) and a HEPA filter (Fig. 1) after the first couple of experiment runs, and had variations in the sample air to clean filtered air ratio, which lead to lower σ_0 in the range

292 of $\sim 1000 - \sim 30000 \text{ Mm}^{-1}$. The system was not always stable, resulting in different measured
293 concentrations for similar sampling times.

294

295 **3.1.1 Particle size distribution**

296 The average size distribution measured with the Grimm 1.108 OPC shows that most particles larger
297 than $1 \mu\text{m}$ (Fig. 2a) were efficiently removed from the air stream with the pre-separator (Fig. 1). This
298 is uncertain, however, since the OPC has been calibrated with white PSL spheres (as discussed in 2.2.3).
299 Another important point is that the lower limit of the sizes the OPC measured was 300 nm , and is
300 probably even higher due to the above-mentioned calibration error. The particle number size
301 distribution, nevertheless, suggests that there were large numbers of BC particles smaller than the OPC
302 detects since the particle number concentration increases sharply with decreasing particle diameter (Fig.
303 2a).

304

305 The mass absorption and scattering coefficients, MAC and MSC, respectively, and single-scattering
306 albedo ω_0 of single BC particles at $\lambda = 530 \text{ nm}$ were modeled with the Mie code of Barber and Hill
307 (1990) and the complex refractive index of $1.85 - 0.71i$ and a particle density of 1.7 g cm^{-3} . Comparison
308 of single-particle ω_0 size distribution (Fig. 2b) with the particle number size distribution (Fig. 2a)
309 suggests ω_0 varied in the range of $\sim 0.3 - 0.5$. Modeling for the size distribution measured with the OPC
310 yielded $\omega_0 \approx 0.51$ and 0.54 when using the original OPC diameters and the diameters multiplied by 2,
311 respectively. These ω_0 values can be considered as upper estimates considering that a large fraction of
312 small particles were undetected. However, to take the ω_0 uncertainty into account we calculated all
313 V2010-related values by using four ω_0 values: 0.3, 0.4, 0.5, and 0.6.

314

315 **3.1.2 Comparison between custom built and commercial PSAPs**

316 The optical depths presented in Svensson et al. (2018) were measured with the custom-made PSAP of
317 Stockholm University at $\lambda = 526 \text{ nm}$, which is slightly different than the commercial Radiance Research
318 PSAP ($\lambda = 530 \text{ nm}$). Therefore, before applying the corrections (determined in section 3.1.3 below) we
319 examined whether the transmittances measured with these two PSAPs agree. Transmittances of all
320 Pallflex and quartz filters were measured with both instruments. The resulting scatter plot (Fig. 3) shows
321 that the agreement is excellent between the PSAPs, thus we concluded that the corrections established
322 in this paper could be applied to the results presented by Svensson et al. (2018).

323

324 **3.1.3 Estimation of the multiple-scattering correction factor C_{ref} for the quartz filter**

325 Optical depths (τ) for both the Pallflex and quartz filters, $\tau(\text{P})$ and $\tau(\text{Q})$, respectively, were calculated
 326 from (5) at a 1-second time resolution. The $\tau(\text{Q})$ -to- $\tau(\text{P})$ ratios – here the τ ratio – got a wide range of
 327 values at 1-second time resolution but most of them were > 1 : 99.6 % of $\tau(\text{Q})/\tau(\text{P}) > 1$ and the average
 328 and median ratios were 1.21 and 1.16, respectively. To study how the τ ratio depends on filter loading
 329 the data were classified into transmittance bins of a 0.025 width in the $\text{Tr}(\text{P})$ range of 0.3 – 1.0 and the
 330 averages and medians were calculated for each bin (shown in Fig. 34). The transmittance dependence
 331 of the τ ratio of individual samples was often controversial: in some samples it decreased from the
 332 beginning, in some samples it increased. We do not have an explanation of this although the high
 333 concentrations in the mixing chamber – see the attenuation coefficients σ_0 in Table 1 – are probably
 334 largely the factor behind this observation. However, for all data the average and median τ ratio depended
 335 on the filter transmittance, so that for a fresh clean filter at $\text{Tr} > 0.9$, it was higher than for heavily-
 336 loaded filters at $\text{Tr} < 0.4$ (Fig. 34). In addition to the 1-second data the τ ratio at the end of each sampling
 337 period are plotted as a function of transmittance of the Pallflex filter in Fig. 34. For the end values of
 338 all samples there was no clear Tr dependence. **The most important conclusion in Fig. 4 is that the τ**
 339 **ratio of the two filter materials depends on the filter transmittance. On the average the ratio decreases**
 340 **with increasing loading even though the same amount of BC is collected on both filters. That suggests**
 341 **that the loading corrections to be applied depend on the filter material and that they do not differ just**
 342 **by a constant factor.**

343
 344 In sample runs 4, 5, 7, 16, 18, 19, and 20 the decrease of Tr was relatively slow and we considered the
 345 bin averages and medians calculated from them to be the most suitable to be used for determining C_{ref} .
 346 Sample 17 was also long, taking more than six minutes. Despite the similar settings used for filling the
 347 mixing chamber and the diluter, the τ ratio was completely different from the rest of the samples (Fig.
 348 34). This outlier was therefore excluded from the analysis.

349
 350 The two correction algorithms (B1999 and V2010) were next applied to both filter materials and $\sigma_{\text{ap}}(\text{Q})$
 351 and $\sigma_{\text{ap}}(\text{P})$ (at $\lambda = 530$ nm) were calculated from (4) by using the Tr bin averages and median of σ_0 and
 352 then the ratio of these two, $\sigma_{\text{ap}}(\text{Q})/\sigma_{\text{ap}}(\text{P})$. When the constants within the correction methods, including
 353 the C_{ref} , were the same for both filter materials the ratio is close to 1.2 (Fig. 45). As mentioned
 354 previously, V2010 depends also on ω_0 , and due to the fact that we are unsure of the ω_0 of the aerosol,
 355 we present four lines ($\omega_0 = 0.3$, $\omega_0 = 0.4$, $\omega_0 = 0.5$, and $\omega_0 = 0.6$) in Fig. 4. The B1999 correction yields
 356 a slightly decreasing $\sigma_{\text{ap}}(\text{Q})/\sigma_{\text{ap}}(\text{P})$, suggesting that only adjusting C_{ref} would not be enough. The V2010
 357 correction does not yield a clear Tr dependence of $\sigma_{\text{ap}}(\text{Q})/\sigma_{\text{ap}}(\text{P})$ although it has high $\sigma_{\text{ap}}(\text{Q})/\sigma_{\text{ap}}(\text{P})$
 358 values in the $\text{Tr}(\text{P})$ range 0.6 – 0.85. They correspond to the local maxima of the average and median τ

359 ratio shown in Fig. 34. Nevertheless, there is not enough data in this study to robustly test the correction
 360 algorithms. Therefore, all values are calculated with both of them. We calculated next the multiple-
 361 scattering correction factor C_{ref} from (7) by using the $Tr(P)$ bin averages of $\sigma_{ap}(Q)/\sigma_{ap}(P)$. The averages
 362 and standard deviations over the $Tr(P,530)$ range of 1 – 0.3 and for averaging of all the four single
 363 scattering albedos $\omega_o = 0.3$, $\omega_o = 0.4$, $\omega_o = 0.5$ and $\omega_o = 0.6$ are presented in Table 2. It is worth noting
 364 that $C_{ref} \approx 3.4$ at $\lambda = 530$ nm is close with published values for another commonly used absorption
 365 photometer, the Aethalometer, that uses quartz filters backed with supporting cellulose fibers. For
 366 instance, values around 3.5 were reported by Segura et al. (2014), Zanatta et al. (2016), and Backman
 367 et al. (2017).

368

369 **3.2 Comparison of τ vs EC of soot mixed in water with airborne particles**

370 The slopes of the optical depths ($f\tau$) vs. EC concentrations, when applying the transmittance-dependent
 371 loading correction $f(Tr,Q,V2010, \omega_o = 0.4)$, were different, and depended on how the soot aerosol were
 372 deposited onto the filter (Fig. 67a and b). For the airborne aerosol, the slope is $6.4 \pm 0.2 \text{ m}^2 \text{ g}^{-1}$; while
 373 the particles mixed in water (without the ultrasonic treatment) have a slope that is doubled (12.6 ± 0.5
 374 $\text{m}^2 \text{ g}^{-1}$). Applying $\omega_o = 0.5$ and $\omega_o = 0.6$ loading corrections, the slopes of the airborne particles are 6.1
 375 $\pm 0.2 \text{ m}^2 \text{ g}^{-1}$ and $5.7 \pm 0.20 \text{ m}^2 \text{ g}^{-1}$, respectively; while the slopes of the particles mixed in water (without
 376 the ultrasonic treatment) are $12.0 \pm 0.4 \text{ m}^2 \text{ g}^{-1}$, and $11.3 \pm 0.4 \text{ m}^2 \text{ g}^{-1}$. The ratios for airborne to liquid
 377 particles are 0.506 ± 0.026 , 0.507 ± 0.026 , and 0.508 ± 0.025 for the three choices of ω_o in the
 378 calculation. The difference in slope between the airborne and liquid particles is likely an effect of
 379 penetration depth of the soot particles into the filter media, with the higher slope for liquid particles
 380 reflecting a deeper penetration. Nevertheless, the ratio is named as the water-mixing factor $f_w \approx 0.51 \pm$
 381 0.03 . In comparison, using $f(Tr,B1999)$ for the airborne and the water-mixed particles the slopes for
 382 optical depth $f\tau$ vs. EC concentration are $4.33 \pm 0.13 \text{ m}^2 \text{ g}^{-1}$ and $8.31 \pm 0.22 \text{ m}^2 \text{ g}^{-1}$, respectively,
 383 providing a ratio of $f_w \approx 0.52 \pm 0.02$, essentially identical to that obtained from the V2010 correction.

384

385 The slope of $f\tau$ vs. EC of the 24 analyzed samples treated in the ultrasonic bath was even higher (Fig.
 386 6a and b), reflecting a probable greater penetration depth of the particles. When $f(Tr,Q,V2010)$ is
 387 calculated with $\omega_o=0.4$, $\omega_o=0.5$ and $\omega_o=0.6$, the slopes of $f\tau$ vs. EC of the particles mixed in water with
 388 the ultrasonic treatment were $18.7 \pm 0.8 \text{ m}^2 \text{ g}^{-1}$, $17.8 \pm 0.8 \text{ m}^2 \text{ g}^{-1}$, and $16.9 \pm 0.7 \text{ m}^2 \text{ g}^{-1}$, respectively.
 389 The average \pm uncertainty of the ratios of the slopes of airborne and water-mixed particles with the
 390 ultrasonic treatment is very stable, 0.34 ± 0.02 . If we consider this value to be a product of a factor f_s
 391 representing the ultrasonic treatment and the above-presented factor f_w we obtain the value $f_s \approx 0.67 \pm$
 392 0.04 . When $f(Tr,B1999)$ is used also for the water-mixed and ultrasonic-bath-treated particles the slope

393 of corrected optical depth $f\tau$ vs. EC concentration is $12.9 \pm 0.4 \text{ m}^2 \text{ g}^{-1}$, with the corresponding $f_s \approx 0.65$
 394 ± 0.03 .

395

396 The factors are used for multiplying $f(\text{Tr}, \text{Q}) = g(\text{Tr})/C_{\text{ref}}(\text{Q})$, and so another way it can be interpreted is
 397 that they affect the multiple scattering correction

398

$$f_s f_w f(\text{Tr}) = \frac{1}{\frac{1}{f_s} \frac{1}{f_w} C_{\text{ref}}} g(\text{Tr})$$

399 In other words, $C_{\text{refSW}}(\text{Q}) = C_{\text{ref}}(\text{Q})/(f_w f_s)$ and $C_{\text{refW}}(\text{Q}) = C_{\text{ref}}(\text{Q})/f_w$ for BC particles mixed in water and
 400 filtered through quartz filters with and without an ultrasonic bath, respectively. The values are presented
 401 in Table 2. The uncertainties of $C_{\text{refW}}(\text{Q})$ and $C_{\text{refSW}}(\text{Q})$ were calculated with a standard error propagation
 402 formula by using the standard deviations of C_{refS} in Table 2 and the above-presented uncertainties of f_w
 403 and f_s .

404

405 To visualize the combined effects of the loading correction functions and the two factors f_w and f_s they
 406 are plotted as a function of τ in Fig. 78. The corresponding transmittances are shown in the secondary
 407 x axis. The range of optical depths of EC in snow presented by Svensson et al. (2018) are also shown
 408 in the figure. It is obvious that the transmittances through those filters were much lower than $\text{Tr} = 0.3$
 409 used in the PSAP calibration in V2010 and even more lower than the $\text{Tr} = 0.6$ recommended in the
 410 World Meteorological Organization and Global Atmosphere Watch (WMO/GAW, 2011) standard
 411 operating procedures. However, since there is no published calibration for such low transmittances and
 412 high optical depths τ the approach of extrapolating is the best that can be done. Figure 78 also shows
 413 how V2010 and B1999 corrections are close to each other at low τ , but for dark filters at $\tau \approx 2$ there is
 414 a factor of ~ 2 difference between them.

415

416 3.3 Implications for field samples

417 Previously published laboratory and ambient τ vs. EC regressions in Svensson et al. (2018), were
 418 updated with the above-developed corrections. Svensson et al. (2018) presented linear regressions of
 419 optical depth τ vs. EC of the same chimney soot we used in the present study, NIST soot (NIST-2975),
 420 and field samples from the Himalaya (India), and Finnish Lapland. ~~However, the optical depths~~
 421 ~~presented by Svensson et al. (2018) were measured with a custom-made PSAP of Stockholm University~~
 422 ~~at $\lambda = 526 \text{ nm}$, not at $\lambda = 530 \text{ nm}$ with the Radiance Research PSAP used in the present study. Therefore,~~
 423 ~~before applying the corrections we examined whether the transmittances measured with these two~~
 424 ~~PSAPs agree. Transmittances of all Pallflex and quartz filters were measured with both instruments.~~
 425 ~~The resulting scatter plot (Fig. 8) shows that the agreement is excellent between the PSAPs, thus we~~

426 ~~concluded that the corrections established in this paper could be done to the results presented by~~
427 ~~Svensson et al. (2018).~~

428

429 We multiplied the τ of the laboratory data of Svensson et al. (2018) with $f_{sfwf}(Tr, V2010, \omega_o=0.4, Q)$
430 since an ultrasonic bath was used also in those experiments. The slopes of the chimney and NIST soot
431 decreased from $\sim 40 \text{ m}^2 \text{ g}^{-1}$ and $\sim 35 \text{ m}^2 \text{ g}^{-1}$ to $11.9 \pm 0.9 \text{ m}^2 \text{ g}^{-1}$ and $9.6 \pm 0.6 \text{ m}^2 \text{ g}^{-1}$, respectively (Fig. 9a
432 and b). In the scatter plot of the chimney soot the two data points with the highest EC concentration of
433 $\sim 0.04 \text{ g m}^{-2}$ are possible outliers. When they are discarded from the regression the slope becomes $9.8 \pm$
434 $0.5 \text{ m}^2 \text{ g}^{-1}$, which is indicated by the red line in Fig. 9a. This is within the uncertainties and is essentially
435 the same as for the NIST soot.

436

437 These values are now in the order of published MACs, but for chimney and NIST soot still considerably
438 larger than the $6.4 \pm 0.2 \text{ m}^2 \text{ g}^{-1}$ obtained in the present work (section 3.2). The explanation to this
439 difference is not clear. However, the procedures of processing the chimney soot and the NIST soot were
440 not exactly identical to the one we used in the present work. Svensson et al. (2018) mixed both types of
441 soot manually in MQ water, added some ethanol in the solution and mixed samples with variable
442 amounts of MQ water before the ultrasonic mixing. In the present work instead, we blew the aerosol
443 through a virtual impactor into the MQ water, took samples of this solution and diluted the samples
444 before the mixing in the ultrasonic bath. The two major differences are the use of the size separation in
445 the present work and the use of ethanol by Svensson et al. (2018), with the explanation being due to
446 those.

447

448 For the re-evaluation of the field data presented by of Svensson et al. (2018) we multiplied the τ with
449 $f_{wf}(Tr, V2010, \omega_o=0.4, Q)$ since the field snow samples were melted and then filtered through the quartz
450 filters. The slopes of the field samples from the Indian Himalaya and from Finnish Lapland decreased
451 from $17.1 \pm 0.8 \text{ m}^2 \text{ g}^{-1}$ and $21.5 \pm 0.8 \text{ m}^2 \text{ g}^{-1}$ to $7.5 \pm 0.4 \text{ m}^2 \text{ g}^{-1}$ and $9.8 \pm 0.5 \text{ m}^2 \text{ g}^{-1}$, respectively (Fig
452 9c and 9d). All slopes above are in the range of published MAC of BC. For instance, **Quinn and Bates**
453 **(2005) obtained MAC values ranging from 6 to 20 $\text{m}^2 \text{ g}^{-1}$, Bond and Bergstrom (2006) and Bond et al.**
454 **(2013) reviewed several articles and according to them the MAC of freshly-generated BC is**
455 **approximately $7.5 \pm 1.2 \text{ m}^2 \text{ g}^{-1}$ at $\lambda = 550 \text{ nm}$.**~~and Quinn and Bates (2005) obtained MAC values ranging~~
456 ~~from 6 to 20 $\text{m}^2 \text{ g}^{-1}$.~~

457

488 **4 Conclusions**

459 Through the airborne laboratory experiments conducted in this study we determined that the multiple
460 scattering effect is enhanced by about 20% with micro quartz filters compared to Pallflex filters. In

461 terms of the multiple-scattering correction factor, C_{ref} , of the quartz filters, we estimate it to be ~3.4 for
462 airborne sampled BC. It is worth noting that this is within the range of C_{ref} values published for the
463 Aethalometer, a very commonly used absorption photometer. The results of the airborne experiments
464 have also other implications. Atmospheric aerosols are often collected on quartz filters and analyzed
465 for EC concentration. The same filter samples can also be used for measuring light absorption to derive
466 the MAC. The analysis showed that if this is done the multiple scattering correction and loading
467 correction should be taken into account, just as they are in the data processing of online aerosol
468 absorption photometers.

469

470 Mixing BC particles in water and filtering the solution essentially doubled the attenuation of light
471 compared to airborne generated filters. This is probably explained by the fact that in the liquid phase
472 and the subsequent filtering the soot particles penetrate deeper into the filter media. Deeper in the filter
473 substrate, it is more likely that the light absorption effects are enhanced, and that way accounting for
474 the measured higher optical depth. In the airborne phase the depositional process is most probably
475 different, with the particulates accumulating in the surface layer of the filter.

476

477 When samples were mixed in an ultrasonic bath before filtering through quartz filters the attenuation
478 was further enhanced. The hypothesis for explaining the effect of the ultrasonic bath is that it possibly
479 breaks the chain-like structure of BC particles, resulting in smaller BC particles that are able to move
480 to further depths in the filter matrix. This remains to be confirmed, and can possibly be done with an
481 electron microscopy. More research on the sampling of BC from melted snow and ice onto filter media
482 is much needed.

483

484 All these effects mean that the absorption data obtained from melted snow samples have high
485 uncertainties. However, application of the correction functions to earlier published field data from the
486 Himalaya and Finnish Lapland yielded MAC values of $\sim 7 - 10 \text{ m}^2 \text{ g}^{-1}$ at $\lambda = 550 \text{ nm}$ which is in the
487 range of published MAC of airborne BC aerosol. This gives indirect support for the validity of the PSAP
488 calibration also for darker filters than used as the limit in atmospheric measurements.

489

490 **Acknowledgements**

491 This work has been supported by the Academy of Finland consortium: “Novel Assessment of Black
492 Carbon in the Eurasian Arctic: From Historical Concentrations and Sources to Future Climate Impacts”
493 (NABCEA project number 296302); and the Academy of Finland project: “Absorbing Aerosols and
494 Fate of Indian Glaciers” (AAFIG; project number 268004). J. Svensson further acknowledges personal
495 support from the Maj and Tor Nessling foundation. J. Ström acknowledges support by the Swedish
496 Research Council (VR 2017-03758) “Black carbon particle size distributions from source to sink.”

497 **References**

- 498 **Arnott, W. P., Hamasha, K., Moosmüller, H., Sheridan, P. J., and Ogren, J. A.:** Towards aerosol light-
499 **absorption measurements with a 7-wavelength aethalometer: Evaluation with a photoacoustic**
500 **instrument and 3-wavelength nephelometer, *Aerosol Sci. Tech.*, 39, 17-29, 2005.**
- 501
- 502 Backman, J., Schmeisser, L., Virkkula, A., Ogren, J. A., Asmi, E., Starkweather, S., Sharma, S.,
503 Eleftheriadis, K., Uttal, T., Jefferson, A., Bergin, M., Makshtas, A., Tunved, P., and Fiebig, M.: On
504 Aethalometer measurement uncertainties and an instrument correction factor for the Arctic, *Atmos.*
505 *Meas. Tech.*, 10, 5039-5062, doi.org/10.5194/amt-10-5039-2017, 2017.
- 506
- 507 Barber, P. W. and Hill, S. C.: *Light scattering by particles: Computational methods*, World Scientific
508 Publishing, Singapore, 1990.
- 509
- 510 Birch, M. E. and Cary R. A.: Elemental carbon-based method for monitoring occupational exposures,
511 to particulate diesel exhaust, *Aerosol Sci. Tech.*, 25, 221–241, 1996.
- 512
- 513 Bond, T. C., Anderson, T. L., and Campbell, D.: Calibration and Intercomparison of Filter-Based
514 Measurements of Visible Light Absorption by Aerosols, *Aerosol Sci. Tech.*, 30, 582–600, 1999.
- 515
- 516 **Bond, T. C., and R. W. Bergstrom: Light absorption by carbonaceous particles: An investigative review,**
517 ***Aerosol Sci. Technol.*, 40(1),27–67, 2006.**
- 518
- 519 Bond, T. C., Doherty, S. J., Fahey, D. W., Forster, P. M., Berntsen, T., DeAngelo, B. J., Flanner, M. G,
520 Ghan, S., Kärcher, B., Koch, D., Kinne, S., Kondo, Y., Quinn, P. K., Sarofim, M. F., Schultz, M. G.,
521 Schulz, M., Venkataraman, C., Zhang, H., Zhang, S., Bellouin, N., Guttikunda, S. K., Hopke, P. K.,
522 Jacobson, M. Z., Kaiser, J. W., Klimont, Z., Lohmann, U., Schwarz, J. P., Shindell, D., Storelvmo, T.,
523 Warren, S. G., and Zender, C. S.: Bounding the role of black carbon in the climate system: A scientific
524 assessment, *J. Geophys. Res.-Atmos.*, 118, 5380–5552, doi.org/10.1002/jgrd.50171, 2013.
- 525
- 526 Cavalli, F., Viana, M., Yttri, K. E., Genberg, J., and Putaud, J.-P.: Toward a standardised thermal-
527 optical protocol for measuring atmospheric organic and elemental carbon: the EUSAAR protocol,
528 *Atmos. Meas. Tech.*, 3, 79–89, doi.org/10.5194/amt-3-79- 2010, 2010.
- 529
- 530 **Collaud Coen, M., Weingartner, E., Apituley, A., Ceburnis, D., Fierz-Schmidhauser, R., Flentje, H.,**
531 **Henzing, J., Jennings, S. G., Moerman, M., and Petzold, A.: Minimizing light absorption measurement**

- 532 artifacts of the Aethalometer: evaluation of five correction algorithms, *Atmos. Meas. Tech.*, 3, 457-474,
533 2010.
- 534
- 535 Delene, D. J. and Ogren, J. A.: Variability of aerosol optical properties at four North American surface
536 monitoring sites, *J. Atmos. Sci.* 59, 1135–1150, 2002.
- 537
- 538 Flanner, M. G., Zender, C. S., Randerson, J. T., and Rasch, P. J.: Present-day climate forcing and
539 response from black carbon in snow, *J. Geophys. Res.-Atmos.*, 112, D11202,
540 doi.org/10.1029/2006JD008003, 2007.
- 541
- 542 Forsström, S., Ström, J., Pedersen, C.A., Isaksson, E., and Gerland, S.: Elemental carbon distribution
543 in Svalbard snow, *J. Geophys. Res.-Atmos.*, 114, D19112, doi:10.1029/2008JD011480, 2009.
- 544
- 545 Hagler, G. S.W., Bergin, M. H., Smith, E. A., Dibb, J. E., Anderson, C., and Steig, E. J.: Particulate and
546 water-soluble carbon measured in recent snow at Summit, Greenland, *Geophys. Res. Lett.*, 34, L16505,
547 doi.org/10.1029/2007GL030110, 2007.
- 548 Gertler, C.G., Puppala, S.P., Panday, A., Stumm, D., Shea, J.: Black carbon and the Himalayan
549 cryosphere: a review. *Atmos. Environ.* 125, 404–417, doi.org/10.1016/j.atmosenv.2015.08.078, 2016.
- 550
- 551 Krecl, P., Ström, J., and Johansson, C.: Carbon content of atmospheric aerosols in a residential area
552 during the wood combustion season in Sweden, *Atmos. Environ.*, 41, 6974–6985, 2007.
- 553
- 554 Meinander, O., Kazadzis, S., Arola, A., Riihelä, A., Räisänen, P., Kivi, R., Kontu, A., Kouznetsov, R.,
555 Sofiev, M., Svensson, J., Suokanerva, H., Aaltonen, V., Manninen, T., Roujean, J.-L., and Hautecoeur,
556 O.: Spectral albedo of seasonal snow during intensive melt period at Sodankylä, beyond the Arctic
557 Circle, *Atmos. Chem. Phys.*, 13, 3793–3810, doi.org/10.5194/acp-13-3793-2013, 2013.
- 558
- 559 Müller, T., Virkkula, A., and Ogren, J. A.: Constrained two-stream algorithm for calculating aerosol
560 light absorption coefficient from the Particle Soot Absorption Photometer, *Atmos. Meas. Tech.*, 7,
561 4049-4070, doi.org/10.5194/amt-7-4049-2014, 2014.
- 562
- 563 Peltoniemi, J. I., Gritsevich, M., Hakala, T., Dagsson-Waldhauserová, P., Arnalds, Ó., Anttila, K.,
564 Hannula, H.-R., Kivekäs, N., Lihavainen, H., Meinander, O., Svensson, J., Virkkula, A., and de Leeuw,
565 G.: Soot on Snow experiment: bidirectional reflectance factor measurements of contaminated snow,
566 *Cryosphere*, 9, 2323-2337, doi.org/10.5194/tc-9-2323-2015, 2015.
- 567

- 568 Ogren, J. A.: Comment on calibration and intercomparison of filter-based measurements of visible light
569 absorption by aerosols, *Aerosol Sci. Tech.*, 44, 589–591, doi.org/10.1080/02786826.2010.482111,
570 2010.
- 571
- 572 Rosenberg, P. D., Dean, A. R., Williams, P. I., Dorsey, J. R., Minikin, A., Pickering, M. A., and Petzold,
573 A.: Particle sizing calibration with refractive index correction for light scattering optical particle
574 counters and impacts upon PCASP and CDP data collected during the Fennec campaign, *Atmos. Meas.*
575 *Tech.*, 5, 1147-1163, doi.org/10.5194/amt-5-1147-2012, 2012.
- 576
- 577 Ruppel, M. M., Isaksson, E., Ström, J., Beaudon, E., Svensson, J., Pedersen, C. A., and Korhola, A.:
578 Increase in elemental carbon values between 1970 and 2004 observed in a 300- year ice core from
579 Holtedahlfonna (Svalbard), *Atmos. Chem. Phys.*, 14, 11447–11460, doi.org/10.5194/acp-14-11447-
580 2014, 2014.
- 581
- 582 Petzold, A., Ogren, J.A., Fiebig, M., Laj, P., Li, S., Baltensperger, U., Holzer-Popp, T., Kinne, S.,
583 Pappalardo, G., Sugimoto, N., Wehrli, C., Wiedensohler, A. and Zhang, X.: Recommendations for
584 reporting black carbon measurements, *Atmos. Chem. Phys.*, 13, 8365–8379, 10.5194/acp-13-8365-
585 2013, 2013.
- 586
- 587 Quinn, P. K. and Bates, T. S.: Regional aerosol properties: comparison of boundary layer measurements
588 from ACE1, ACE2, Aerosols99, INDOEX, ACE Asia, TARFOX, and NEAQS, *J. Geophys. Res.*, 110,
589 D14202, doi:10.1029/2004JD004755, 2005.
- 590
- 591 Segura, S., Estellés, V., Titos, G., Lyamani, H., Utrillas, M.P., Zotter, P., Prévôt, A.S.H., Močnik, G.,
592 Alados-Arboledas, L., and Martínez-Lozano, J.A.: Determination and analysis of in situ spectral aerosol
593 optical properties by a multi-instrumental approach. *Atmos. Meas. Tech.* 7, 2373–2387,
594 doi.org/10.5194/amt-7-2373-2014, 2014.
- 595
- 596 **Schwarz, J. P., Gao, R. S., Perring, A. E., Spackman, J. R., and Fahey, D. W.: Black carbon aerosol size**
597 **in snow, *Nat. Sci. Reports*, 3, 1356, <https://doi.org/10.1038/srep01356>, 2013.**
- 598
- 599 Skiles, S. M., Flanner, M., Cook, J. M., Dumont, M., and Painter, T. H.: Radiative forcing by light-
600 absorbing particles in snow, *Nat. Clim. Change*, 8, 964–971, doi.org/10.1038/s41558-018- 0296-5,
601 2018.
- 602
- 603 Svensson, J., Virkkula, A., Meinander, O., Kivekäs, N., Hannula, H.-R., Järvinen, O., Peltoniemi, J. I.,
604 Gritsevich, M., Heikkilä, A., Kontu, A., Neitola, K., Brus, D., Dagsson-Waldhauserova, P., Anttila, K.,

- 605 Vehkamäki, M., Hienola, A., de Leeuw, G., and Lihavainen, H.: Soot-doped natural snow and its albedo
606 – results from field experiments, *Boreal Environ. Res.*, 21, 481–503, 2016.
- 607
- 608 Svensson, J., Ström, J., Kivekäs, N., Dkhar, N. B., Tayal, S., Sharma, V. P., Jutila, A., Backman, J.,
609 Virkkula, A., Ruppel, M., Hyvärinen, A., Kontu, A., Hannula, H.-R., Leppäranta, M., Hooda, R. K.,
610 Korhola, A., Asmi, E., and Lihavainen, H.: Light-absorption of dust and elemental carbon in snow in
611 the Indian Himalayas and the Finnish Arctic, *Atmos. Meas. Tech.*, 11, 1403-1416, doi.org/10.5194/amt-
612 11-1403-2018, 2018.
- 613
- 614 Virkkula, A.: Correction of the calibration of the 3-wavelength Particle Soot Absorption Photometer
615 (3 λ PSAP), *Aerosol Sci. Tech.*, 44, 706–712, doi.org/10.1080/02786826.2010.482110, 2010.
- 616
- 617 Virkkula, A., Ahlquist, N. C., Covert, D. S., Arnott, W. P., Sheridan, P. J., Quinn, P. K., and Coffman,
618 D. J.: Modification, calibration and a field test of an instrument for measuring light absorption by
619 particles, *Aerosol Sci. Tech.*, 39, 68–83, doi.org/10.1080/027868290901963, 2005.
- 620
- 621 Warren, S. and Wiscombe, W.: A model for the spectral albedo of snow II. Snow containing
622 atmospheric aerosols, *J. Atmos. Sci.*, 37, 2734–2745, 1980.
- 623
- 624 WMO/GAW: WMO/GAW Standard Operating Procedures for In-situ Measurements of Aerosol Mass
625 Concentration, Light Scattering and Light Absorption, GAW Report No. 200, World Meteorological
626 Organization, Geneva, Switzerland, 2011.
- 627
- 628 Xu, B., Cao, J., Hansen, J., Yao, T., Joswiak, D.R., Wang, N., Wu, G., Wang, M., Zhao, H., Yang, W.,
629 Liu, X., and He, J.: Black soot and the survival of Tibetan glaciers. *Proc. Nat. Acad. Sci. USA*, 106,
630 22114–22118, doi:10.1073/pnas.0910444106, 2009.
- 631
- 632 Zanatta, M., Gysel, M., Bukowiecki, N., Müller, T., Weingartner, E., Areskoug, H., Fiebig, M., Yttri,
633 K.E., Mihalopoulos, N., Kouvarakis, G., Beddows, D., Harrison, R.M., Cavalli, F., Putaud, J.P.,
634 Spindler, G., Wiedensohler, A., Alastuey, A., Pandolfi, M., Sellegri, K., Swietlicki, E., Jaffrezo, J.L.,
635 Baltensperger, U., and Laj, P.: A European aerosol phenomenology-5: climatology of black carbon
636 optical properties at 9 regional background sites across Europe. *Atmos. Environ.* 145, 346–364,
637 doi.org/10.1016/j.atmosenv.2016.09.035, 2016.
- 638
- 639 Zhang, Y., Kang, S., Li, C., Gao, T., Cong, Z., Sprenger, M., Liu, Y., Li, X., Guo, J., Sillanpää, M.,
640 Wang, K., Chen, J., Li, Y., and Sun, S.: Characteristics of black carbon in snow from Laohugou No. 12

Quartz filter characterization with soot tests

641 glacier on the northern Tibetan Plateau, *Sci. Total Environ.*, 607–608, 1237–1249,
642 doi.org/10.1016/j.scitotenv.2017.07.100, 2017.

643 Table 1. Main information on aerosol samples taken during the experiment. Sampling time, Tr:
 644 transmittances of Pallflex and quartz filters at $\lambda = 530$ nm at the end of each sample, σ_0 : attenuation
 645 coefficient, calculated without any loading corrections, $\tau(Q)/\tau(P)$: ratio of optical depths of quartz and
 646 Pallflex filters and EC: EC concentration in the quartz filter. The 1-second data from samples denoted
 647 with * were used for deriving C_{ref} of quartz filters. Samples 1 and 2 were taken from the mixing chamber
 648 without any dilution.

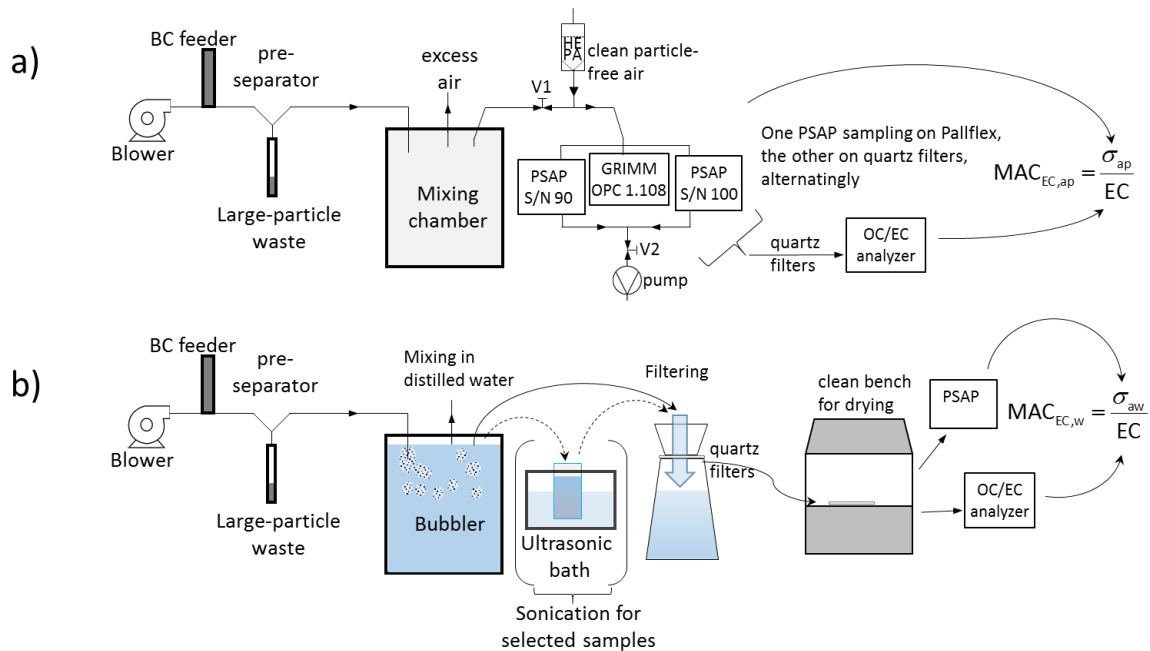
Sample number	Sampling time min			$\sigma_0(P)$	$\sigma_0(Q)$	$\tau(Q)/\tau(P)$	EC g m ⁻²
		Tr(P)	Tr(Q)	Mm ⁻¹	Mm ⁻¹		
1	0.55	0.314	0.279	84245	92840	1.102	0.172
2	0.43	0.493	0.458	65284	72082	1.104	0.113
3	1.82	0.544	0.487	13405	15842	1.182	0.094
4*	6.7	0.543	0.509	3646	4032	1.106	0.056
5*	11.8	0.746	0.702	993	1199	1.207	0.029
6	2.68	0.543	0.505	9103	10184	1.119	0.062
7*	12.13	0.224	0.216	4932	5052	1.024	0.195
8	0.6	0.609	0.592	33062	34950	1.057	0.027
9	0.88	0.823	0.797	8821	10275	1.165	0.014
10	0.67	0.913	0.902	5461	6188	1.133	0.016
11	1.38	0.931	0.923	2067	2317	1.121	0.027
12	0.32	0.915	0.904	11221	12749	1.136	0.012
13	0.57	0.927	0.913	5351	6425	1.201	0.009
14	0.65	0.814	0.781	12664	15211	1.201	0.011
15	2.93	0.704	0.664	4786	5584	1.167	0.032
16*	11.6	0.602	0.555	1750	2030	1.16	0.029
17	6.12	0.5	0.415	4533	5751	1.269	0.080
18*	11.92	0.401	0.354	3067	3486	1.136	0.113
19*	10.47	0.302	0.262	4576	5119	1.119	0.147
20*	6.97	0.402	0.367	5232	5755	1.1	0.113
21	3.6	0.6	0.558	5676	6482	1.142	0.055
22	2.1	0.849	0.833	3118	3480	1.116	0.017

649
 650 Table 2. Multiple-scattering correction factors of quartz filters. $C_{ref}(Q)$: derived here for airborne BC
 651 particles from published Pallflex filter loading corrections V2010 and O2010. $C_{refW}(Q)$: derived here
 652 for BC particles mixed in water and filtered through quartz filters. $C_{refSW}(Q)$: derived here for BC
 653 particles mixed in water and treated in an ultrasonic bath and filtered through quartz filters.

	Derived from V2010			Derived from O2010
	467 nm	530 nm	660 nm	same for all λ
$C_{ref}(Q)$	3.23 ± 0.04	3.41 ± 0.03	3.48 ± 0.09	3.08 ± 0.04
$C_{refW}(Q)$	6.4 ± 0.3	6.7 ± 0.3	6.9 ± 0.4	5.9 ± 0.2
$C_{refSW}(Q)$	9.5 ± 0.7	10.0 ± 0.8	10.2 ± 0.8	9.1 ± 0.6

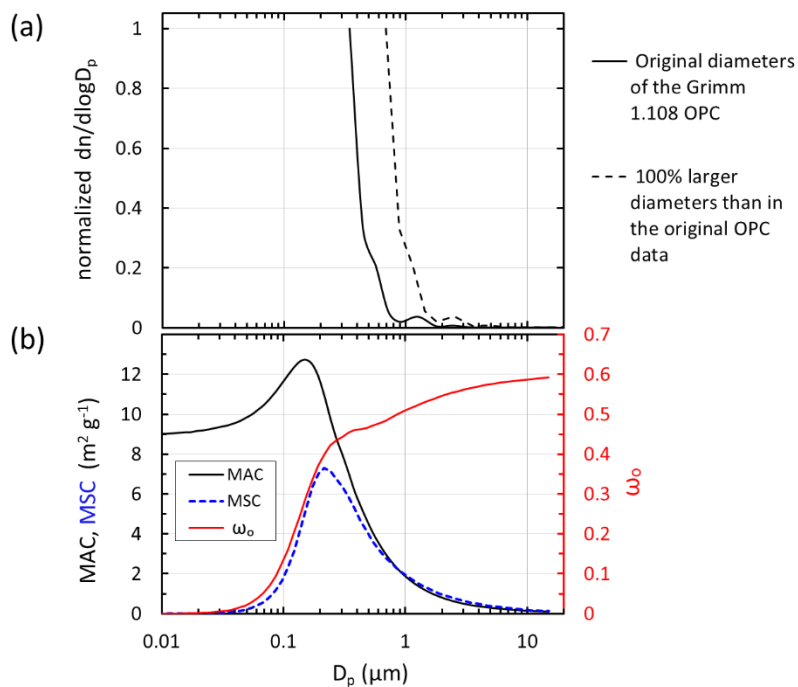
654
 655

656 **Figures**



657

658 Figure 1. Experimental setup for the airborne (a), and for the liquid (b) procedures.

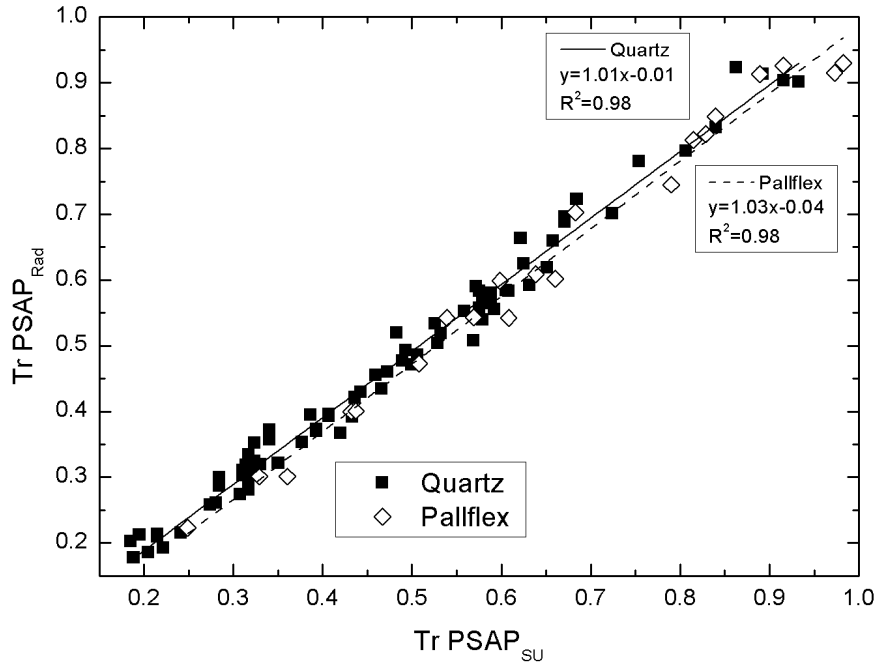


659

660 Figure 2. Size-dependent aerosol properties relevant to the experiment. a) Normalized average particle
 661 number size distribution of soot aerosol measurement in the mixing chamber with the Grimm 1.108
 662 OPC. The continuous lines present the size distributions with the original diameters of the OPC and the
 663 dashed lines those assuming that the original diameters were underestimated by a factor of 2. b) Mass
 664 absorption and scattering coefficients, MAC and MSC, respectively, and single-scattering albedo ω_0 of
 665 single BC particles at $\lambda = 530 \text{ nm}$.

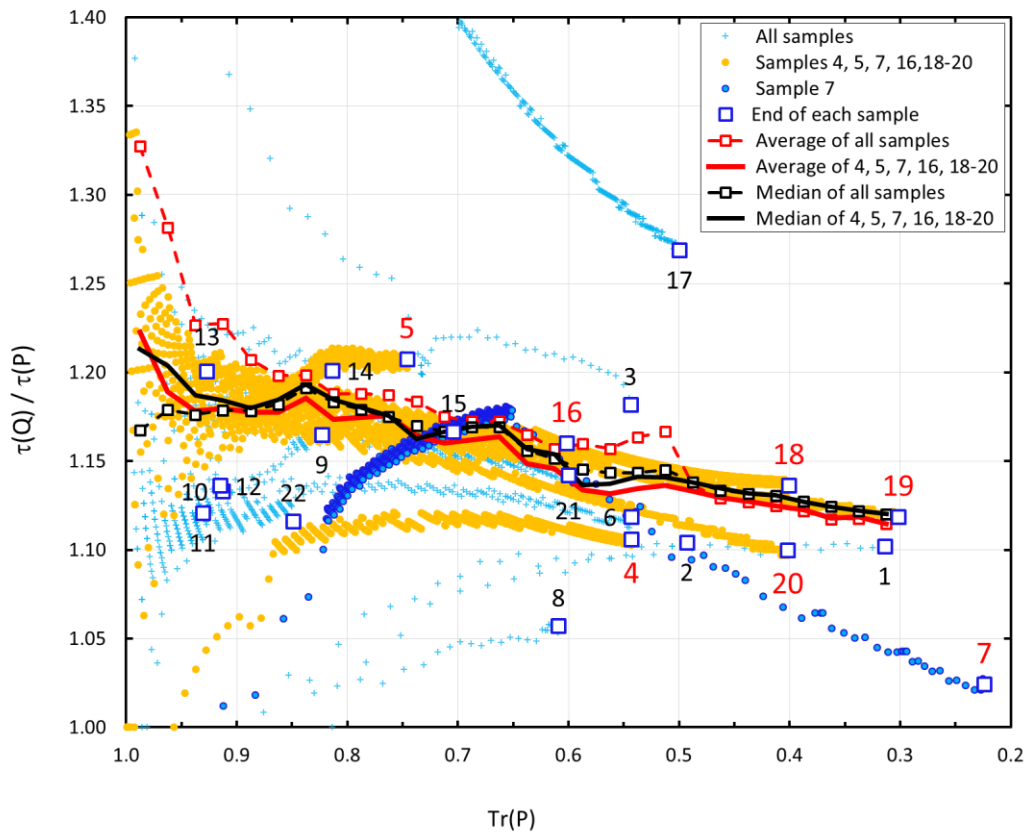
666

Quartz filter characterization with soot tests



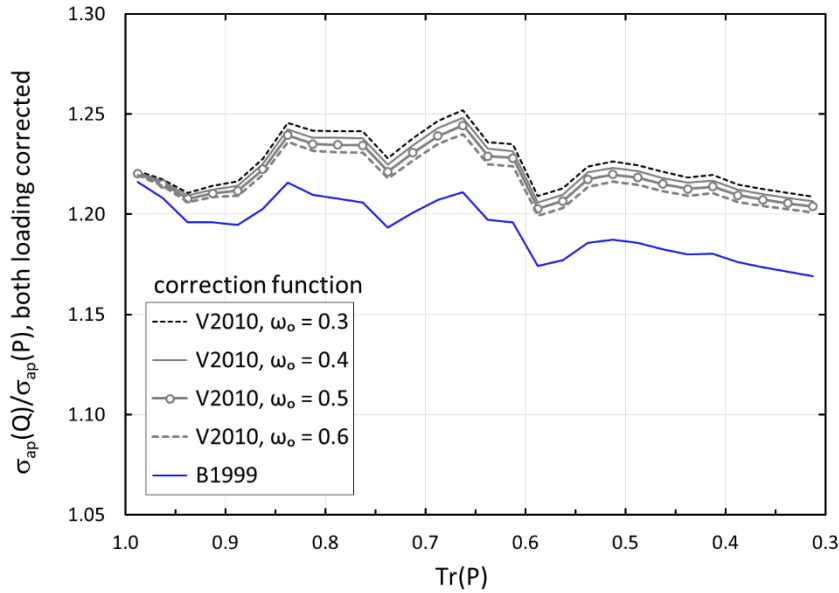
667
668
669
670
671

Figure 3. Transmittance for quartz and Pallflex filters measured with PSAP radiance research and the Stockholm University custom-built PSAP.

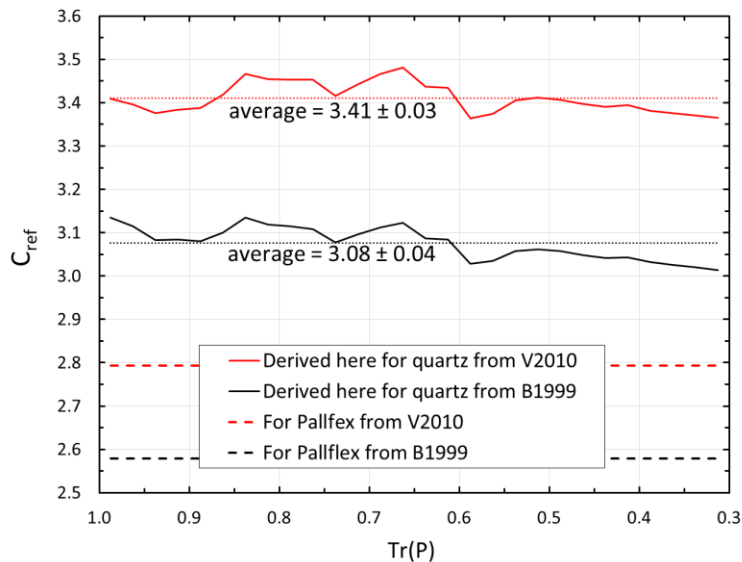


672

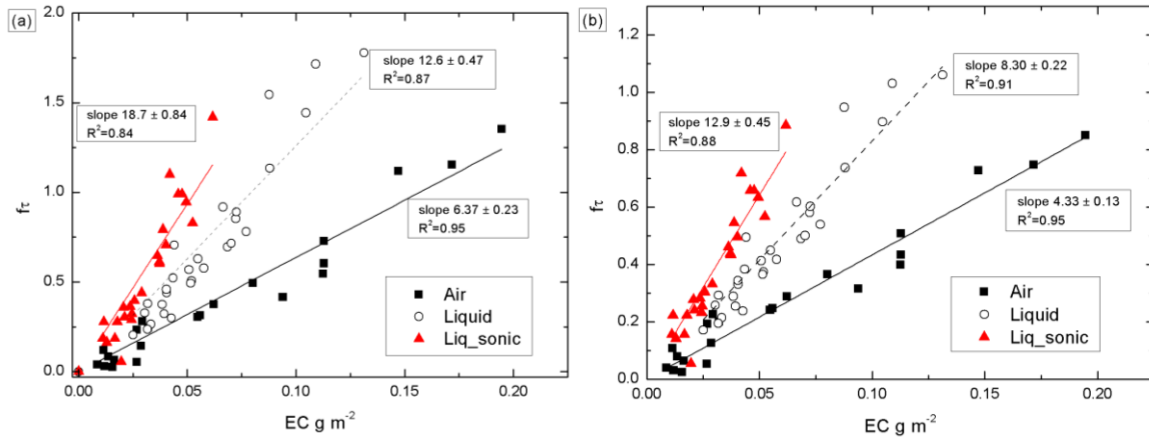
673 Figure 34. Ratio of non-loading-corrected optical depths ($\tau = \ln(1/\text{Tr})$) of quartz and Pallflex filters,
 674 $\tau(Q)$ and $\tau(P)$, respectively at $\lambda = 530$ nm at one second time resolution.. The numbers denote the value
 675 at the end of each sample. The red numbers are associated with those samples that were used for deriving
 676 $C_{\text{ref}}(\text{quartz})$ in section 3.1.2



677
 678 Figure 45. Average $\sigma_{\text{ap}}(\text{quartz})/\sigma_{\text{ap}}(\text{Pallflex})$ in 0.025 bins of transmittance of Pallflex filter at $\lambda = 530$
 679 nm. Both $\sigma_{\text{ap}}(\text{quartz})$ and $\sigma_{\text{ap}}(\text{Pallflex})$ were corrected both either according to Bond et al. (1999) with
 680 the Ogren (2010) modification (O2010) and Virkkula (2010) (V2010) using four values for the single-
 681 scattering albedo ω_o .

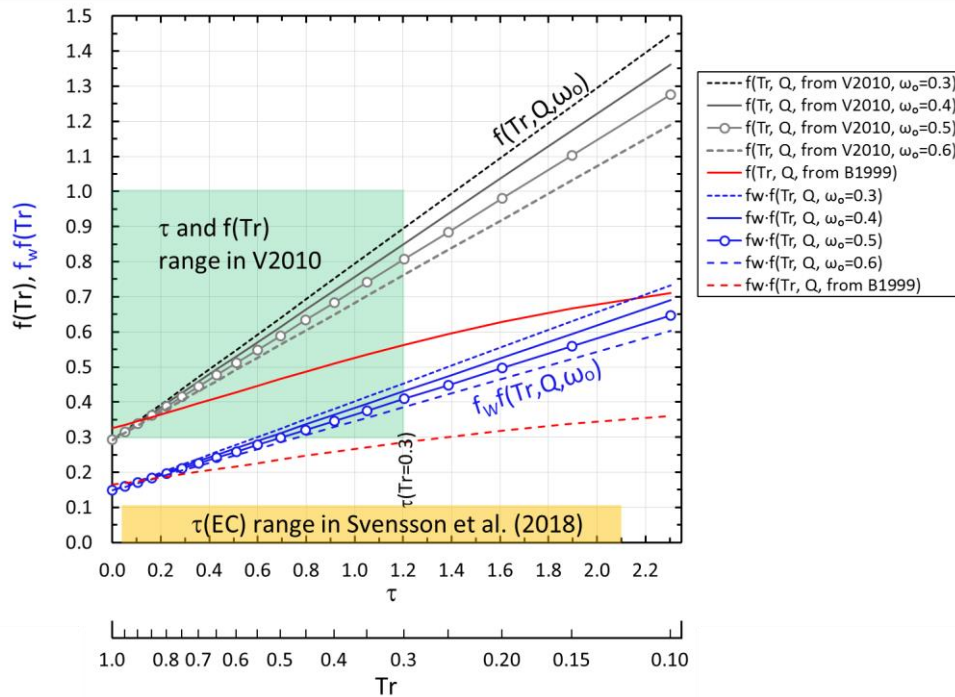


682
 683 Figure 56. The multiple-scattering correction factor C_{ref} for quartz and Pallflex filters in 0.025 bins of
 684 transmittance of Pallflex filter at $\lambda = 530$ nm. The straight lines for C_{ref} of O2010 and V2010 are those
 685 shown in Eqs. (9) and (12).
 686



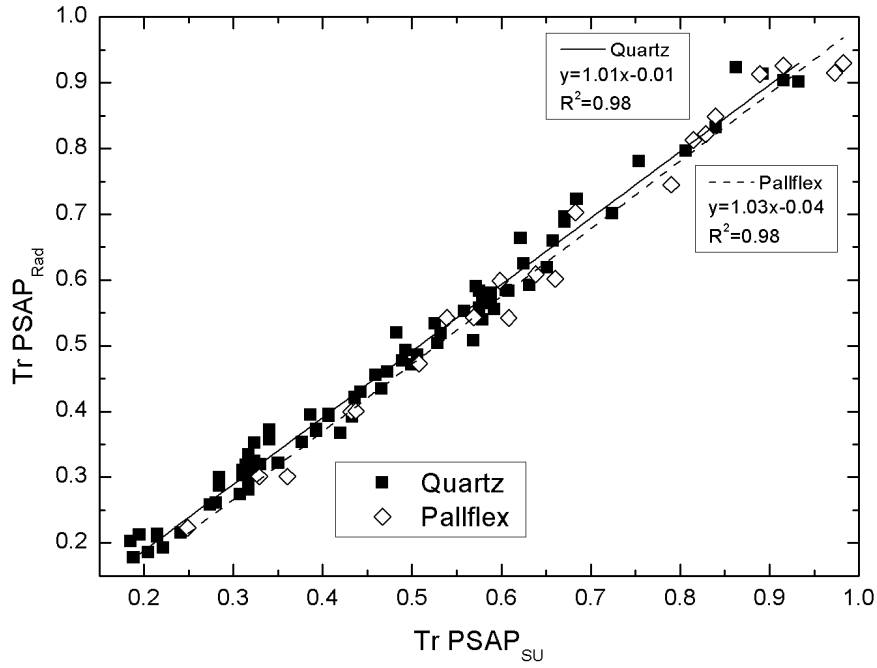
687
688
689
690
691
692
693

Figure 67. Linear regressions of transmittance-corrected optical depth $f\tau(\lambda = 530 \text{ nm})$ vs. EC of the BC particles blown into the mixing chamber (Air), into water (Liquid) and blown into water and treated in the ultrasonic bath (Liq_sonic). The optical depths were corrected with a) the $f(\text{Tr}, \text{V2010}, \omega_0=0.4)$ and b) $f(\text{Tr}, \text{Q}, \text{O2010})$. The regressions were calculated by forcing offset to 0.



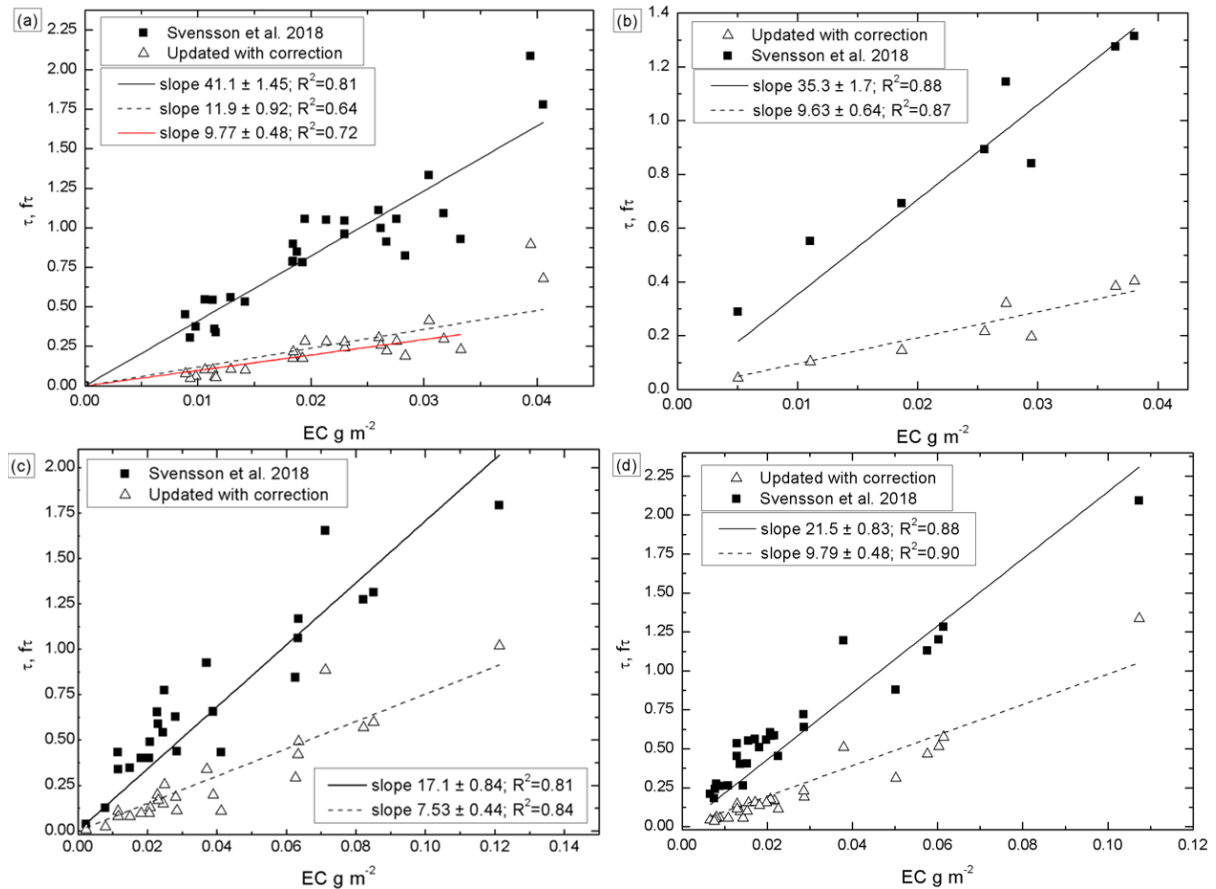
694
695
696
697
698
699

Figure 78. Loading correction functions derived from V2010 and O2010 for airborne BC particles collected on quartz filters (grey lines, $f(\text{Tr}, \text{Q}, \omega_0)$) and for BC particles mixed in water and filtered through similar quartz filters (blue lines, $f_w f(\text{Tr}, \text{Q}, \omega_0)$). The green shadowed area shows the range of optical depths and $f(\text{Tr})$ of the V2010 Pallflex filter calibration and the yellow shadowed line shows the range of optical depths of EC in snow presented by Svensson et al. (2018).



700
701
702
703

Figure 8. Transmittance for quartz and Pallflex filters measured with PSAP radiance research and the Stockholm University custom built PSAP.



704
705

706 Figure 9. Reanalysis of linear regressions presented by Svensson et al. (2018). a) chimney soot, with
707 the red line showing the slope with the two points with the highest EC content are excluded, b) NIST
708 soot, c) field samples from the Indian Himalaya, d) field samples from Finnish Lapland. On the x axis
709 there is the EC concentration as g m^{-2} and on the y axis the non-corrected and corrected optical depth,
710 τ and $f\tau$, respectively.